

Observation of inclusive $B \rightarrow X_s \eta$ at Belle

I. Adachi,¹⁰ H. Aihara,⁵⁹ K. Arinstein,^{1,41} T. Aso,⁶³ V. Aulchenko,^{1,41} T. Aushev,^{26,19}
 T. Aziz,⁵⁴ S. Bahinipati,³ A. M. Bakich,⁵³ V. Balagura,¹⁹ Y. Ban,⁴⁵ E. Barberio,³⁰
 A. Bay,²⁶ I. Bedny,^{1,41} K. Belous,¹⁶ V. Bhardwaj,⁴⁴ B. Bhuyan,¹³ M. Bischofberger,³³
 S. Blyth,³⁵ A. Bondar,^{1,41} A. Bozek,³⁷ M. Bračko,^{28,20} J. Brodzicka,³⁷ T. E. Browder,⁹
 M.-C. Chang,⁴ P. Chang,³⁶ Y.-W. Chang,³⁶ Y. Chao,³⁶ A. Chen,³⁴ K.-F. Chen,³⁶
 P.-Y. Chen,³⁶ B. G. Cheon,⁸ C.-C. Chiang,³⁶ R. Chistov,¹⁹ I.-S. Cho,⁶⁵ S.-K. Choi,⁷
 Y. Choi,⁵² J. Crnkovic,¹² J. Dalseno,^{29,55} M. Danilov,¹⁹ A. Das,⁵⁴ M. Dash,⁶⁴
 A. Drutskoy,³ W. Dungen,¹⁵ S. Eidelman,^{1,41} D. Epifanov,^{1,41} M. Feindt,²² H. Fujii,¹⁰
 M. Fujikawa,³³ N. Gabyshev,^{1,41} A. Garmash,^{1,41} G. Gokhroo,⁵⁴ P. Goldenzweig,³
 B. Golob,^{27,20} M. Grosse Perdekamp,^{12,47} H. Guo,⁴⁹ H. Ha,²³ J. Haba,¹⁰ B.-Y. Han,²³
 K. Hara,³¹ T. Hara,¹⁰ Y. Hasegawa,⁵¹ N. C. Hastings,⁵⁹ K. Hayasaka,³¹ H. Hayashii,³³
 M. Hazumi,¹⁰ D. Heffernan,⁴³ T. Higuchi,¹⁰ Y. Horii,⁵⁸ Y. Hoshi,⁵⁷ K. Hoshina,⁶²
 W.-S. Hou,³⁶ Y. B. Hsiung,³⁶ H. J. Hyun,²⁵ Y. Igarashi,¹⁰ T. Iijima,³¹ K. Inami,³¹
 A. Ishikawa,⁴⁸ H. Ishino,^{60,*} K. Itoh,⁵⁹ R. Itoh,¹⁰ M. Iwabuchi,⁶ M. Iwasaki,⁵⁹ Y. Iwasaki,¹⁰
 T. Jinno,³¹ M. Jones,⁹ N. J. Joshi,⁵⁴ T. Julius,³⁰ D. H. Kah,²⁵ H. Kakuno,⁵⁹ J. H. Kang,⁶⁵
 P. Kapusta,³⁷ S. U. Kataoka,³² N. Katayama,¹⁰ H. Kawai,² T. Kawasaki,³⁹ A. Kibayashi,¹⁰
 H. Kichimi,¹⁰ C. Kiesling,²⁹ H. J. Kim,²⁵ H. O. Kim,²⁵ J. H. Kim,⁵² S. K. Kim,⁵⁰
 Y. I. Kim,²⁵ Y. J. Kim,⁶ K. Kinoshita,³ B. R. Ko,²³ S. Korpar,^{28,20} M. Kreps,²²
 P. Križan,^{27,20} P. Krokovny,¹⁰ T. Kuhr,²² R. Kumar,⁴⁴ T. Kumita,⁶¹ E. Kurihara,²
 E. Kuroda,⁶¹ Y. Kuroki,⁴³ A. Kusaka,⁵⁹ A. Kuzmin,^{1,41} Y.-J. Kwon,⁶⁵ S.-H. Kyeong,⁶⁵
 J. S. Lange,⁵ G. Leder,¹⁵ M. J. Lee,⁵⁰ S. E. Lee,⁵⁰ S.-H. Lee,²³ J. Li,⁹ A. Limosani,³⁰
 S.-W. Lin,³⁶ C. Liu,⁴⁹ D. Liventsev,¹⁹ R. Louvot,²⁶ J. MacNaughton,¹⁰ F. Mandl,¹⁵
 D. Marlow,⁴⁶ A. Matyja,³⁷ S. McOnie,⁵³ T. Medvedeva,¹⁹ Y. Mikami,⁵⁸ K. Miyabayashi,³³
 H. Miyake,⁴³ H. Miyata,³⁹ Y. Miyazaki,³¹ R. Mizuk,¹⁹ A. Moll,^{29,55} T. Mori,³¹ T. Müller,²²
 R. Mussa,¹⁸ T. Nagamine,⁵⁸ Y. Nagasaka,¹¹ Y. Nakahama,⁵⁹ I. Nakamura,¹⁰ E. Nakano,⁴²
 M. Nakao,¹⁰ H. Nakayama,⁵⁹ H. Nakazawa,³⁴ Z. Natkaniec,³⁷ K. Neichi,⁵⁷ S. Neubauer,²²
 S. Nishida,¹⁰ K. Nishimura,⁹ O. Nitoh,⁶² S. Noguchi,³³ T. Nozaki,¹⁰ A. Ogawa,⁴⁷
 S. Ogawa,⁵⁶ T. Ohshima,³¹ S. Okuno,²¹ S. L. Olsen,⁵⁰ W. Ostrowicz,³⁷ H. Ozaki,¹⁰
 P. Pakhlov,¹⁹ G. Pakhlova,¹⁹ H. Palka,³⁷ C. W. Park,⁵² H. Park,²⁵ H. K. Park,²⁵
 K. S. Park,⁵² L. S. Peak,⁵³ M. Pernicka,¹⁵ R. Pestotnik,²⁰ M. Peters,⁹ L. E. Piilonen,⁶⁴
 A. Poluektov,^{1,41} K. Prothmann,^{29,55} B. Riesert,²⁹ M. Rozanska,³⁷ H. Sahoo,⁹
 K. Sakai,³⁹ Y. Sakai,¹⁰ N. Sasao,²⁴ O. Schneider,²⁶ P. Schönmeier,⁵⁸ J. Schümann,¹⁰
 C. Schwanda,¹⁵ A. J. Schwartz,³ R. Seidl,⁴⁷ A. Sekiya,³³ K. Senyo,³¹ M. E. Seviar,³⁰
 L. Shang,¹⁴ M. Shapkin,¹⁶ V. Shebalin,^{1,41} C. P. Shen,⁹ H. Shibuya,⁵⁶ S. Shiizuka,³¹
 S. Shinomiya,⁴³ J.-G. Shiu,³⁶ B. Shwartz,^{1,41} F. Simon,^{29,55} J. B. Singh,⁴⁴ R. Sinha,¹⁷
 A. Sokolov,¹⁶ E. Solovieva,¹⁹ S. Stanič,⁴⁰ M. Starič,²⁰ J. Stypula,³⁷ A. Sugiyama,⁴⁸
 K. Sumisawa,¹⁰ T. Sumiyoshi,⁶¹ S. Suzuki,⁴⁸ S. Y. Suzuki,¹⁰ Y. Suzuki,³¹ F. Takasaki,¹⁰
 N. Tamura,³⁹ K. Tanabe,⁵⁹ M. Tanaka,¹⁰ N. Taniguchi,¹⁰ G. N. Taylor,³⁰ Y. Teramoto,⁴²
 I. Tikhomirov,¹⁹ K. Trabelsi,¹⁰ Y. F. Tse,³⁰ T. Tsuboyama,¹⁰ K. Tsunada,³¹ Y. Uchida,⁶
 S. Uehara,¹⁰ Y. Ueki,⁶¹ K. Ueno,³⁶ T. Uglov,¹⁹ Y. Unno,⁸ S. Uno,¹⁰ P. Urquijo,³⁰

Y. Ushiroda,¹⁰ Y. Usov,^{1,41} G. Varner,⁹ K. E. Varvell,⁵³ K. Vervink,²⁶ A. Vinokurova,^{1,41}
C. C. Wang,³⁶ C. H. Wang,³⁵ J. Wang,⁴⁵ M.-Z. Wang,³⁶ P. Wang,¹⁴ X. L. Wang,¹⁴
M. Watanabe,³⁹ Y. Watanabe,²¹ R. Wedd,³⁰ J.-T. Wei,³⁶ J. Wicht,¹⁰ L. Widhalm,¹⁵
J. Wiechczynski,³⁷ E. Won,²³ B. D. Yabsley,⁵³ H. Yamamoto,⁵⁸ Y. Yamashita,³⁸
M. Yamauchi,¹⁰ C. Z. Yuan,¹⁴ Y. Yusa,⁶⁴ C. C. Zhang,¹⁴ L. M. Zhang,⁴⁹ Z. P. Zhang,⁴⁹
V. Zhilich,^{1,41} V. Zhulanov,^{1,41} T. Zivko,²⁰ A. Zupanc,²⁰ N. Zwahlen,²⁶ and O. Zyukova^{1,41}

(The Belle Collaboration)

¹*Budker Institute of Nuclear Physics, Novosibirsk*

²*Chiba University, Chiba*

³*University of Cincinnati, Cincinnati, Ohio 45221*

⁴*Department of Physics, Fu Jen Catholic University, Taipei*

⁵*Justus-Liebig-Universität Gießen, Gießen*

⁶*The Graduate University for Advanced Studies, Hayama*

⁷*Gyeongsang National University, Chinju*

⁸*Hanyang University, Seoul*

⁹*University of Hawaii, Honolulu, Hawaii 96822*

¹⁰*High Energy Accelerator Research Organization (KEK), Tsukuba*

¹¹*Hiroshima Institute of Technology, Hiroshima*

¹²*University of Illinois at Urbana-Champaign, Urbana, Illinois 61801*

¹³*India Institute of Technology Guwahati, Guwahati*

¹⁴*Institute of High Energy Physics,*

Chinese Academy of Sciences, Beijing

¹⁵*Institute of High Energy Physics, Vienna*

¹⁶*Institute of High Energy Physics, Protvino*

¹⁷*Institute of Mathematical Sciences, Chennai*

¹⁸*INFN - Sezione di Torino, Torino*

¹⁹*Institute for Theoretical and Experimental Physics, Moscow*

²⁰*J. Stefan Institute, Ljubljana*

²¹*Kanagawa University, Yokohama*

²²*Institut für Experimentelle Kernphysik, Universität Karlsruhe, Karlsruhe*

²³*Korea University, Seoul*

²⁴*Kyoto University, Kyoto*

²⁵*Kyungpook National University, Taegu*

²⁶*École Polytechnique Fédérale de Lausanne (EPFL), Lausanne*

²⁷*Faculty of Mathematics and Physics, University of Ljubljana, Ljubljana*

²⁸*University of Maribor, Maribor*

²⁹*Max-Planck-Institut für Physik, München*

³⁰*University of Melbourne, School of Physics, Victoria 3010*

³¹*Nagoya University, Nagoya*

³²*Nara University of Education, Nara*

³³*Nara Women's University, Nara*

³⁴*National Central University, Chung-li*

³⁵*National United University, Miao Li*

³⁶*Department of Physics, National Taiwan University, Taipei*

³⁷*H. Niewodniczanski Institute of Nuclear Physics, Krakow*

³⁸*Nippon Dental University, Niigata*

- ³⁹*Niigata University, Niigata*
⁴⁰*University of Nova Gorica, Nova Gorica*
⁴¹*Novosibirsk State University, Novosibirsk*
⁴²*Osaka City University, Osaka*
⁴³*Osaka University, Osaka*
⁴⁴*Panjab University, Chandigarh*
⁴⁵*Peking University, Beijing*
⁴⁶*Princeton University, Princeton, New Jersey 08544*
⁴⁷*RIKEN BNL Research Center, Upton, New York 11973*
⁴⁸*Saga University, Saga*
⁴⁹*University of Science and Technology of China, Hefei*
⁵⁰*Seoul National University, Seoul*
⁵¹*Shinshu University, Nagano*
⁵²*Sungkyunkwan University, Suwon*
⁵³*School of Physics, University of Sydney, NSW 2006*
⁵⁴*Tata Institute of Fundamental Research, Mumbai*
⁵⁵*Excellence Cluster Universe, Technische Universität München, Garching*
⁵⁶*Toho University, Funabashi*
⁵⁷*Tohoku Gakuin University, Tagajo*
⁵⁸*Tohoku University, Sendai*
⁵⁹*Department of Physics, University of Tokyo, Tokyo*
⁶⁰*Tokyo Institute of Technology, Tokyo*
⁶¹*Tokyo Metropolitan University, Tokyo*
⁶²*Tokyo University of Agriculture and Technology, Tokyo*
⁶³*Toyama National College of Maritime Technology, Toyama*
⁶⁴*IPNAS, Virginia Polytechnic Institute and State University, Blacksburg, Virginia 24061*
⁶⁵*Yonsei University, Seoul*

Abstract

We report on the first observation of inclusive $B \rightarrow X_s \eta$ decays using a sample of $657 \times 10^6 B\bar{B}$ pairs accumulated at the $\Upsilon(4S)$ resonance with the Belle detector at the KEKB asymmetric e^+e^- collider. The X_s system is a charmless inclusive state with unit strangeness, and is reconstructed using a pseudo-inclusive technique from a kaon and up to four pions, of which at most one pion is neutral. We measure a partial branching fraction for $M_{X_s} < 2.6 \text{ GeV}/c^2$ to be $(25.5 \pm 2.7(\text{stat}) \pm 1.6(\text{syst})_{-14.1}^{+3.8}(\text{model})) \times 10^{-5}$. A significant fraction of this signal occurs in the region $M_{X_s} > 1.8 \text{ GeV}/c^2$, which is beyond the range of all previously measured exclusive contributions to $B \rightarrow X_s \eta$.

PACS numbers:

Charmless B decays involve $b \rightarrow s$ penguin transitions that provide sensitivity for precision tests of the Standard Model and searches for new physics. Decays of this type that involve the η and η' mesons exhibit unique properties due to interference effects between their underlying pseudoscalar octet and singlet components [1]. Although these mixing effects are now relatively well understood in the exclusive $B \rightarrow K^{(*)}\eta^{(\prime)}$ decays, the picture is less clear in the modes $B \rightarrow X_s\eta^{(\prime)}$, where X_s is an inclusive state of unit strangeness recoiling against the $\eta^{(\prime)}$.

The CLEO collaboration first reported observation of $B \rightarrow X_s\eta'$ in 1998, and found a larger than expected branching fraction, with an X_s spectrum that peaks at high recoil mass [2]. These findings were confirmed in improved measurements by CLEO and BaBar [3, 4]. Both the high decay rate and the rise at high X_s mass were first attributed to the QCD anomaly mechanism, which couples two gluons to the singlet component of the η' [5]. Other explanations included an intrinsic charm component of the η' , or large contributions from non-perturbative charming penguin amplitudes [6, 7]. The first two explanations are disfavored by existing data [8, 9], while the latter requires more data to confirm.

A measurement of the complementary process $B \rightarrow X_s\eta$ may clarify the situation, as η - η' mixing suggests that mechanisms with couplings to the pseudoscalar singlet, η_0 , should be significant in the η' mode but less so in the mode with an η . A previous search for $B \rightarrow X_s\eta$ was performed by CLEO with $3.3 \times 10^6 B\bar{B}$ pairs, but was only able to place an unrestrictive upper limit of $\mathcal{B}(B \rightarrow X_s\eta) < 4.4 \times 10^{-4}$ [2]. We report the results of a search using a significantly larger dataset. This analysis is based on a sample of $657 \times 10^6 B\bar{B}$ pairs collected with the Belle detector at the KEKB asymmetric e^+e^- collider [10].

The Belle detector is a large-solid-angle magnetic spectrometer that consists of a silicon vertex detector (SVD), a 50-layer central drift chamber (CDC), an array of aerogel threshold Cherenkov counters (ACC), a barrel-like arrangement of time-of-flight scintillation counters (TOF), and an electromagnetic calorimeter (ECL) comprised of CsI(Tl) crystals located inside a superconducting solenoid coil that provides a 1.5 T magnetic field. An iron flux-return located outside of the coil is instrumented to detect K_L^0 mesons and to identify muons (KLM). The detector is described in detail elsewhere [11]. Two inner detector configurations were used. A 2.0 cm beampipe and a 3-layer silicon vertex detector was used for the first sample of $152 \times 10^6 B\bar{B}$ pairs, while a 1.5 cm beampipe, a 4-layer silicon detector and a small-cell inner drift chamber were used to record the remaining $505 \times 10^6 B\bar{B}$ pairs [12].

We reconstruct candidate B mesons using a pseudo-inclusive method, with the X_s reconstructed as a K^+ or K_S^0 and up to four pions, of which at most one is a π^0 . This gives a total of 18 reconstructed channels and their charge conjugates [13]:

$$\begin{array}{ll}
B^+ \rightarrow K^+(\pi^0)\eta & B^0 \rightarrow K_S^0(\pi^0)\eta \\
B^+ \rightarrow K_S^0\pi^+(\pi^0)\eta & B^0 \rightarrow K^+\pi^-(\pi^0)\eta \\
B^+ \rightarrow K^+\pi^+\pi^-(\pi^0)\eta & B^0 \rightarrow K_S^0\pi^+\pi^-(\pi^0)\eta \\
B^+ \rightarrow K_S^0\pi^+\pi^-\pi^+(\pi^0)\eta & B^0 \rightarrow K^+\pi^-\pi^+\pi^-(\pi^0)\eta \\
B^+ \rightarrow K^+\pi^+\pi^-\pi^+\pi^-\eta & B^0 \rightarrow K_S^0\pi^+\pi^-\pi^+\pi^-\eta
\end{array}$$

Candidate η mesons are reconstructed in the $\eta \rightarrow \gamma\gamma$ mode from photons with $E_\gamma > 200$ MeV. The invariant mass of the γ -pair is required to lie between 480 MeV/ c^2 and 620 MeV/ c^2 . We veto an η candidate if either of its photons can be combined with another photon in the event to form a candidate π^0 . To suppress possible backgrounds from radiative B decays, we require the energy asymmetry of the two photons, defined as $|E_{\gamma_1} - E_{\gamma_2}|/|E_{\gamma_1} + E_{\gamma_2}|$, be less than 0.6. The momenta of η candidates meeting these

requirements are recalculated using the nominal η mass. To suppress contamination from $b \rightarrow c$ decays in which the subsequent decay of the charm meson may produce an η , we retain only η candidates whose center-of-mass (CM) momentum satisfies $|\mathbf{p}_\eta^*| > 1.6 \text{ GeV}/c$.

Charged pion and kaon selection is based on a likelihood ratio, $\mathcal{L}_K/(\mathcal{L}_K + \mathcal{L}_\pi)$, which includes information from the TOF and ACC systems, as well as ionization loss measurements from the CDC. A track is identified as a kaon (pion) if the likelihood ratio is greater than 0.6 (less than 0.9). K_S^0 candidates are reconstructed from pairs of oppositely charged tracks whose invariant mass lies within $16 \text{ MeV}/c^2$ of the K_S^0 mass. The vertex of the pair must be well reconstructed and displaced from the interaction point, and the reconstructed K_S^0 momentum vector must be aligned with the $\pi^+\pi^-$ vertex vector.

π^0 candidates are reconstructed from γ -pairs, with the energy requirement $E_\gamma > 50 \text{ MeV}$ in the barrel region and $E_\gamma > 100 \text{ MeV}$ in the endcap region. To reduce misreconstructed photons, we require that 90% of the energy of each γ candidate be contained within the central 3×3 array of calorimeter crystals within the 5×5 array of crystals used to reconstruct the photon. The π^0 momentum is refitted with its mass fixed to the nominal π^0 mass. We require π^0 candidates to have laboratory momenta greater than $300 \text{ MeV}/c$.

Pions and kaons are combined to form an X_s . To reduce the large number of potential candidates, we keep only those with $M_{X_s} < 3.0 \text{ GeV}/c^2$. B meson candidates are then formed from combinations of η and X_s . A beam constrained mass, $M_{bc} = \sqrt{E_{\text{beam}}^2/c^4 - |\mathbf{p}_B^*|^2/c^2}$ and energy difference, $\Delta E = E_B - E_{\text{beam}}$ are calculated, where E_{beam} , \mathbf{p}_B^* , and E_B are the beam energy, B momentum, and B energy, all in the CM frame. We retain B candidates with $M_{bc} > 5.23 \text{ GeV}/c^2$ and $|\Delta E| < 0.5 \text{ GeV}$. We define the fit region for signal extraction with the tighter criteria $|\Delta E| < 0.1 \text{ GeV}$, $|\mathbf{p}_\eta^*| > 2.0 \text{ GeV}/c$, and $520 \text{ MeV}/c^2 < M_\eta < 570 \text{ MeV}/c^2$. The signal region is the subset of the fit region with the added requirement of $M_{bc} > 5.27 \text{ GeV}/c^2$.

To estimate efficiency of these selection criteria, we use a combined signal Monte Carlo (MC) sample consisting of $B \rightarrow K\eta$ for $M_{X_s} < 0.6 \text{ GeV}/c^2$, $B \rightarrow K^*\eta$ for $0.8 \text{ GeV}/c^2 < M_{X_s} < 1.0 \text{ GeV}/c^2$, and $B \rightarrow X_s\eta$ in all other mass regions ($0.6 \text{ GeV}/c^2 < M_{X_s} < 0.8 \text{ GeV}/c^2$, and $M_{X_s} > 1.0 \text{ GeV}/c^2$). For the $B \rightarrow X_s\eta$ MC samples, fragmentation of the X_s system into hadrons is performed by PYTHIA [14, 15], assuming a model in which the X_s mass spectrum is flat from the $K\pi$ threshold up to $3.2 \text{ GeV}/c^2$. From this combined signal MC sample, we find an average of approximately nine B candidates per event. In events with multiple candidates, we select the candidate with the lowest $\chi^2 = \chi_{\text{vtx}}^2 + \chi_{\Delta E}^2$, where χ_{vtx}^2 is the reduced- χ^2 of a vertex fit which includes all charged tracks except those used as part of a K_S^0 candidate, and $\chi_{\Delta E}^2 = \Delta E/\sigma_{\Delta E}$. The resolution, $\sigma_{\Delta E}$, is estimated separately for each reconstructed mode using the signal MC. In the case where there are fewer than two charged tracks available for vertex fitting, only $\chi_{\Delta E}^2$ is used to select the best candidate. Within the signal region, this procedure selects a correctly reconstructed B in 80% of events.

The dominant background to $B \rightarrow X_s\eta$ comes from continuum production of quark pairs, $e^+e^- \rightarrow q\bar{q}$ ($q = u, d, s, c$). These events have a jet-like topology, and are suppressed relative to the spherical $B\bar{B}$ events using a Fisher discriminant [16] formed from 16 modified Fox-Wolfram moments [17, 18], the cosine of the center-of-momentum angle between the reconstructed B flight direction and the axis anti-parallel to the positron beam, $\cos\theta_B$, and, if available, the displacement between the signal B and the other B in the event, Δz . This suppression is optimized as a function of b -flavor tag quality [19], and is approximately 34% efficient for the signal modes while suppressing over 99% of the continuum background.

Decays of the type $B \rightarrow X_c \eta$ and $B \rightarrow X_c \rightarrow X_s \eta$, where X_c is any state including mesons with charm quarks, may have final states identical to the signal mode. Although these backgrounds are largely suppressed by the requirement of a high momentum η , we apply vetoes to further reduce these contributions. We search within the candidate B decay products for combinations consistent with selected charm meson decays and veto the candidate if the mass of the reconstructed combination is within 2.5σ of the relevant mass. We add one extra veto for possible contamination from $\eta' \rightarrow \eta\pi^+\pi^-$. Candidates are vetoed if the high momentum η can be combined with any pair of oppositely charged pions from the event to give an invariant mass $M_{\eta\pi\pi}$ consistent with an η' . The full list of vetoed modes and mass ranges is given in Table I.

TABLE I: List of reconstructed modes used to veto charm and η' decays, along with the mass width over which the veto is applied.

Reconstruction for Veto	Veto Width (MeV/ c^2)
$D^0 \rightarrow Kn\pi^\pm$	± 13.5
$D^0 \rightarrow Kn\pi^\pm\pi^0$	± 44.5
$D^+ \rightarrow Kn\pi^\pm$	± 12.5
$D^+ \rightarrow Kn\pi^\pm\pi^0$	± 12.5
$D^0 \rightarrow K_S^0\eta$	± 31.3
$D_s^+ \rightarrow \eta\pi^+$	± 29.3
$\eta_c(1S) \rightarrow \eta\pi^+\pi^-$	± 85
$\eta' \rightarrow \eta\pi^+\pi^-$	± 100

Signal yields are obtained using an extended unbinned maximum likelihood fit to M_{bc} over the fit region in 200 MeV/ c^2 bins of X_s mass spanning the range $0.4 \text{ GeV}/c^2 < M_{X_s} < 2.6 \text{ GeV}/c^2$. The probability distribution function (PDF) for the signal is taken as a Gaussian, with the mean and width determined from the appropriate signal MC sample ($K\eta$, $K^*\eta$, or $X_s\eta$) for the mass bin. Shapes for the charm contributions that remain after the vetoes are assigned based on an MC sample of generic $b \rightarrow c$ processes. The four largest charm backgrounds identified in MC are assigned separate PDFs: $B^0 \rightarrow \bar{D}^0\eta$, $B^0 \rightarrow \bar{D}^{*0}\eta$, $B^0 \rightarrow D^{(*)-}\pi^+\eta$, and $B^+ \rightarrow \bar{D}^{(*)0}\pi^+\eta$. All other $b \rightarrow c$ backgrounds are combined into another PDF. Each PDF for charm backgrounds consists of a Gaussian plus an ARGUS [20] function. All shape parameters are taken from the appropriate background MC sample. Normalization of the color suppressed modes $B^0 \rightarrow \bar{D}^{(*)0}\eta$ is based on a previous Belle measurement [21]. The branching fractions for the three body decays, $B \rightarrow D^{(*)}\pi\eta$, are entirely unknown, so their normalization is determined by minimization of a χ^2 based on the difference between the expected and observed M_{bc} distributions in all eight veto windows simultaneously. This χ^2 is minimized with respect to the relative normalizations of $B^0 \rightarrow D^{(*)-}\pi^+\eta$ and $B^+ \rightarrow \bar{D}^{(*)0}\pi^+\eta$. The relative normalizations of $D^-\pi^+\eta$ and $D^{*-}\pi^+\eta$ are assumed to be identical, and likewise for the $D^{(*)0}$ modes. Normalization for the PDF that includes all other $b \rightarrow c$ modes is fixed to the MC expectation. The remaining combinatorial $q\bar{q}$ backgrounds are modeled with an ARGUS function.

For the final fit, the signal yield and both the yield and shape parameter of the combinatorial background function are allowed to vary. A small contamination in signal yield from the decays $B \rightarrow X_s\eta'$, $B \rightarrow X_s\gamma$, and $B \rightarrow X_d\eta$ is identified using an MC sample

of rare B decays. These expected yields are subtracted from the fit yield to give a final yield. The fit yields following this subtraction are shown in bins of X_s mass in Figure 1. Two combined fits are also performed for the mass ranges $1.0 \text{ GeV}/c^2 < M_{X_s} < 2.6 \text{ GeV}/c^2$ and $1.8 \text{ GeV}/c^2 < M_{X_s} < 2.6 \text{ GeV}/c^2$, in order to isolate the signal contributions above the known exclusive $K^*\eta$, $K_0^*(1430)\eta$, and $K_2^*(1430)\eta$ signals. Fits to these regions are shown in Figure 2, and give a background subtracted yield of 749 ± 48 (stat) ± 7 (syst) and 244 ± 34 (stat) ± 3 (syst), respectively. Systematic errors included in these yields are those due to $b \rightarrow c$ background modeling, background subtractions, and fitting. In the lower X_s mass bins below $1.4 \text{ GeV}/c^2$, the background subtraction for the $B \rightarrow X_d\eta$ is the largest contribution. Since these modes are rare and relatively poorly measured, we estimate the error by varying the expected yield from MC by $\pm 100\%$. This yield is usually between 1-2 events, except in the lowest mass bin, $0.4 \text{ GeV}/c^2 < M_{X_s} < 0.6 \text{ GeV}/c^2$, where it peaks at 5 events. In the M_{X_s} bins above $1.4 \text{ GeV}/c^2$, the error is dominated by the $b \rightarrow c$ modeling. To calculate this uncertainty, we allow the normalizations of the five $b \rightarrow c$ PDFs to vary. For the three body $B \rightarrow D^{(*)}\pi\eta$ modes, we allow the normalization to vary within the errors determined from the χ^2 minimization procedure used to determine the level of these backgrounds. In the case of the remaining color suppressed PDFs and the PDF that includes all other $b \rightarrow c$ backgrounds, we allow the normalization to vary up to the difference between that used for the fit and that which would be obtained if the normalization were allowed to vary during the χ^2 minimization procedure. The error in yield due to these variations is approximately 2-3 events in all bins above $1.4 \text{ GeV}/c^2$. Errors due to the fitting procedure are estimated by allowing the signal PDF parameters to vary by $\pm 1\sigma$, and are less than 1 event in all bins.

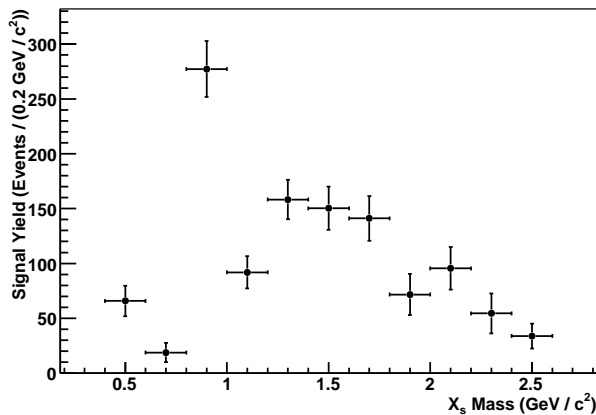


FIG. 1: Background subtracted yields from M_{bc} fits in bins of M_{X_s} . Error bars include statistical errors and systematic errors related to the fitting and background subtraction procedures.

The branching fraction is calculated using M_{X_s} -bin dependent efficiencies obtained from the MC samples of $K\eta$, $K^*\eta$, and $X_s\eta$ with a flat mass distribution. The detection efficiency, including $\mathcal{B}(K_S^0 \rightarrow \pi^+\pi^-)$ and modes that are not reconstructed, but not $\mathcal{B}(\eta \rightarrow \gamma\gamma)$, is 6.5% in the lowest M_{X_s} bin and decreases to 0.12% in the highest bin. Using this efficiency we calculate a partial branching fraction of

$$\mathcal{B}(B \rightarrow X_s\eta; M_{X_s} < 2.6 \text{ GeV}/c^2) = (25.5 \pm 2.7 \text{ (stat)} \pm 1.6 \text{ (syst)}_{-14.1}^{+3.8} \text{ (model)}) \times 10^{-5}.$$

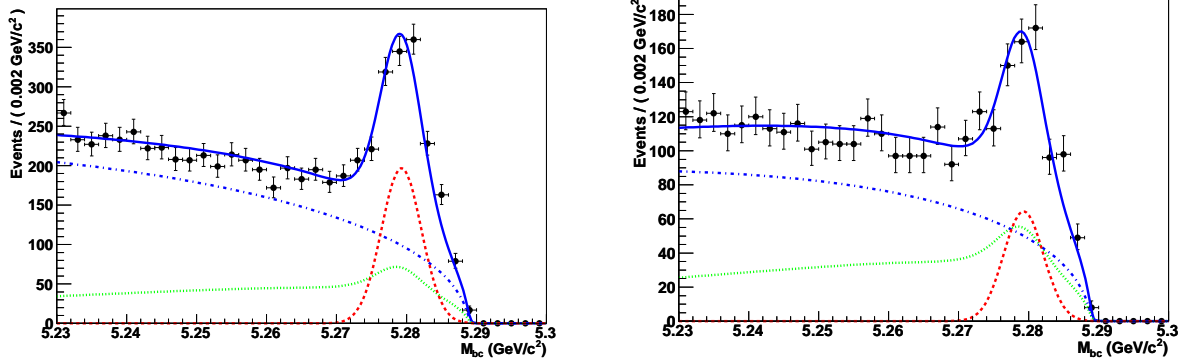


FIG. 2: Fits to M_{bc} for the combined mass range $1.0 \text{ GeV}/c^2 < M_{X_s} < 2.6 \text{ GeV}/c^2$ (left) and $1.8 \text{ GeV}/c^2 < M_{X_s} < 2.6 \text{ GeV}/c^2$ (right). The points with errors are data, the total fit function is shown in solid blue, and the individual fit components for signal, generic backgrounds, and combinatorial background are shown in dashed red, dotted green, and dash-dotted blue, respectively.

In addition to the previously described systematic errors on the background subtracted yields, the systematic error for this result also includes effects of tracking, charged particle identification, the continuum suppression requirements, the candidate selection, the branching fraction of $\eta \rightarrow \gamma\gamma$, identification of η , K_S^0 , and π^0 mesons, and the uncertainty in the total number of $B\bar{B}$ pairs in the data sample. The largest error of approximately 4% in all mass bins comes from the continuum suppression requirements. This error is evaluated using differences between data and Monte Carlo efficiencies in a $B \rightarrow D\pi^\pm$ control sample, with the D meson reconstructed in the same way as an X_s . Tracking and η reconstruction are the next largest, and contribute no more than 2-3% each in all bins. The total systematic error due to these effects rises from 5.6% in the lowest mass bin to 6.3% in the highest mass bin.

Systematic errors due to modeling of the MC events are quoted separately from other systematic errors. We evaluated them for the PYTHIA fragmentation, unreconstructed or "missing" modes, and the X_s spectrum modeling. Of these, the dominant error is due to the uncertainty from PYTHIA fragmentation of the X_s system. To estimate this effect, we refit the data for $M_{X_s} > 1.0 \text{ GeV}/c^2$, divided into subsamples: modes with charged or neutral B mesons, modes with K_S^0 or K^\pm , modes with total pion multiplicity of 1-2 or 3-4, and modes with or without a π^0 . We then compare the yields for each of these categories to those expected from the PYTHIA MC expectation. In all cases the data yields are consistent with those expected from PYTHIA, except in the case of the modes with or without a π^0 , where we find $(57 \pm 13)\%$ of the expected PYTHIA yield in π^0 modes. Therefore, we reweight the PYTHIA-based efficiency to agree with data, and use the difference between this efficiency and the unmodified PYTHIA efficiency as a conservative modeling error due to fragmentation. This error is applied only for bins where we assume a PYTHIA fragmentation model, and ranges from 23% to 73%, with the error generally increasing with M_{X_s} . In addition to the fragmentation error, the modeling systematic also includes an error for unreconstructed, or "missing," modes and mass migration between M_{X_s} bins due to choice of the MC M_{X_s} shape and migration between M_{X_s} bins. For the missing mode estimation, we allow the fraction of missing modes assumed in the MC to vary by 30%, except for modes that are unreconstructed only due to the presence of a K_L^0

rather than a K_S^0 . This results in a systematic error that steadily increases from less than 1% in the lowest bin to 21% in the highest bin. To estimate the effects of mass migration between bins as well as the assumption of a flat mass spectrum, we generate two other signal models where the shape of M_{X_s} is calculated using the QCD anomaly model with η' swapped for η , and a model based on three-body phase space for $b \rightarrow sd\eta$ or $b \rightarrow sun\eta$, with the strange and light quark fragmented by PYTHIA. We study each model in Monte Carlo and determine the difference between the assumed efficiency and the efficiency for candidates reconstructed only in the correct M_{X_s} bin. This difference is calculated for all three models, and the maximum difference of the three models is used as a systematic error. This gives a systematic error of 11% or less in all bins.

The differential branching fraction, including all statistical and systematic errors, is shown in Figure 3. We check our results for consistency with the known $B \rightarrow K\eta$ using the lowest mass bin, and find a branching fraction of $(2.0 \pm 0.4 \pm 0.2) \times 10^{-6}$, which agrees with previous Belle measurements [22, 23]. We also check the bin between 0.8 and 1.0 GeV/c^2 , and find a branching fraction of $(1.77 \pm 0.14 \pm 0.10) \times 10^{-5}$, which is in good agreement with the $B \rightarrow K^*\eta$ world average [24]. A direct comparison to the known $B \rightarrow K_{0,2}^*(1430)\eta$ rates [25] is less straightforward due to overlap effects and larger widths. We measure a significant previously unobserved signal above 1.8 GeV/c^2 , where contributions from these known modes are negligible. We also note that the rise in spectrum toward high X_s mass bears a strong resemblance to that of $B \rightarrow X_s\eta'$ [3, 4].

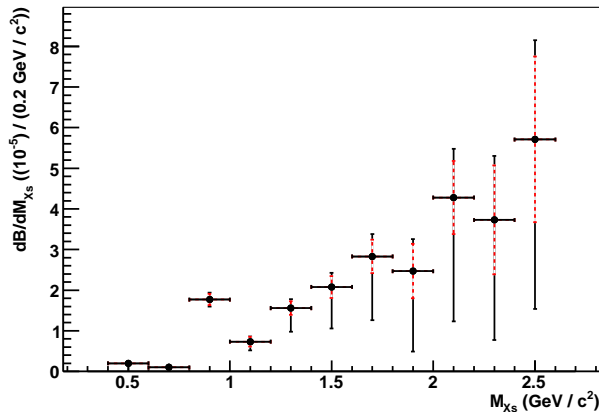


FIG. 3: Differential branching fraction, $d\mathcal{B}/dM_{X_s}$, for $B \rightarrow X_s\eta$. Dashed red error bars are statistical only, solid black error bars include all systematic and modeling errors.

In conclusion, we have made the first measurement of the inclusive partial branching fraction for $B \rightarrow X_s\eta$, and find $\mathcal{B}(B \rightarrow X_s\eta; 0.4 \text{ GeV}/c^2 < M_{X_s} < 2.6 \text{ GeV}/c^2) = (25.5 \pm 2.7 \text{ (stat)} \pm 1.6 \text{ (syst)}_{-14.1}^{\text{(model)}}) \times 10^{-5}$. We also report a differential branching fraction that rises at high X_s mass.

No theoretical prediction is currently available for the M_{X_s} mass, so no direct comparison can be made. However, the similarity in spectral shape to $B \rightarrow X_s\eta'$, as well as the lack of strong suppression of the $B \rightarrow X_s\eta$ branching fraction relative to the η' mode, implies that the $\eta'gg$ coupling originally used to explain the $B \rightarrow X_s\eta'$ signal is strongly disfavored. Rather, recent work suggests that the relative strengths of the two processes is due to a large contribution of charming penguin amplitudes in both decays [7].

We thank the KEKB group for the excellent operation of the accelerator, the KEK cryogenics group for the efficient operation of the solenoid, and the KEK computer group and the National Institute of Informatics for valuable computing and SINET3 network support. We acknowledge support from the Ministry of Education, Culture, Sports, Science, and Technology of Japan and the Japan Society for the Promotion of Science; the Australian Research Council and the Australian Department of Education, Science and Training; the National Natural Science Foundation of China under contract No. 10575109 and 10775142; the Department of Science and Technology of India; the BK21 program of the Ministry of Education of Korea, the CHEP SRC program and Basic Research program (grant No. R01-2005-000-10089-0) of the Korea Science and Engineering Foundation, and the Pure Basic Research Group program of the Korea Research Foundation; the Polish State Committee for Scientific Research; the Ministry of Education and Science of the Russian Federation and the Russian Federal Agency for Atomic Energy; the Slovenian Research Agency; the Swiss National Science Foundation; the National Science Council and the Ministry of Education of Taiwan; and the U.S. Department of Energy.

* now at Okayama University, Okayama

- [1] H.J. Lipkin, Phys. Lett. B **254**, 247 (1991).
- [2] T.E. Browder *et al.* (CLEO Collaboration), Phys. Rev. Lett. **81**, 1786 (1998).
- [3] G. Bonvicini *et al.* (CLEO Collaboration), Phys. Rev. D **68**, 011101 (2003).
- [4] B. Aubert *et al.* (BaBar Collaboration), Phys. Rev. Lett. **93**, 061801 (2004).
- [5] D. Atwood and A. Soni, Phys. Lett. B **405**, 150 (1997).
- [6] I. E. Halperin and A. Zhitnitsky, Phys. Rev. Lett. **80**, 438 (1998).
- [7] J. Chay, C. Kim, A. K. Leibovich, and J. Zupan, Phys. Rev. D **74**, 092005 (2007).
- [8] M. Artuso *et al.* (CLEO Collaboration), Phys. Rev. D **67**, 052003 (2003).
- [9] K. W. Edwards *et al.* (CLEO Collaboration), Phys. Rev. Lett. **86**, 30 (2001).
- [10] S. Kurokawa and E. Kikutani, Nucl. Instr. Meth. A **499**, 1 (2003).
- [11] A. Abashian *et al.* (Belle Collaboration), Nucl. Instr. Meth. A **479**, 117 (2002).
- [12] Z. Natkaniec *et al.* (Belle SVD2 Group), Nucl. Instr. Meth. A **560**, 1 (2006).
- [13] Throughout this paper, the inclusion of the charge conjugate mode decay is implied unless otherwise stated.
- [14] We use the EvtGen B meson decay generator, D.J. Lange, Nucl. Instr. Meth. A **462**, 152 (2001). The detector response is simulated with GEANT, R. Brun *et al.*, GEANT 3.21, CERN Report DD/EE/84-1 (1984).
- [15] T. Sjostrand, S. Mrenna, and P. Skands, JHEP **05**, 026 (2006).
- [16] R. A. Fisher, Annals of Eugenics **7**, 179 (1936).
- [17] “SFW”: The Fox-Wolfram moments were introduced in G. C. Fox and S. Wolfram, Phys. Rev. Lett. **41**, 1581 (1978). The Fisher discriminant used by Belle, based on modified Fox-Wolfram moments (SFW), is described in K. Abe *et al.* (Belle Collaboration), Phys. Rev. Lett. **87**, 101801 (2001) and K. Abe *et al.* (Belle Collaboration), Phys. Lett. B **511**, 151 (2001).
- [18] “KSFW”: S. H. Lee *et al.* (Belle Collaboration), Phys. Rev. Lett. **91**, 261801 (2003).
- [19] “Flavor Tagging”: H. Kakuno *et al.*, Nucl. Instr. Meth. A **533**, 516 (2004).
- [20] H. Albrecht *et al.* (ARGUS Collaboration), Phys. Lett. B **241**, 278 (1990).
- [21] S. Blyth *et al.* (Belle Collaboration), Phys. Rev. D **74**, 092002 (2006).

- [22] K. Abe *et al.* (Belle Collaboration), Phys. Lett. B **662**, 323 (2008).
- [23] K. Abe *et al.* (Belle Collaboration), Phys. Rev. D **75**, 071104 (2007).
- [24] C. Amsler *et al.* (Particle Data Group), Phys. Lett. B **667**, 1 (2008).
- [25] B. Aubert *et al.* (BaBar Collaboration), Phys. Rev. Lett. **97**, 201802 (2006).